Models of Coastally Trapped Disturbances

WILLIAM C. SKAMAROCK, RICHARD ROTUNNO, AND JOSEPH B. KLEMP

National Center for Atmospheric Research, Boulder, Colorado*

(Manuscript received 11 March 1998, in final form 10 November 1998)

ABSTRACT

During the spring and summer, the climatological northerly flow along the U.S. west coast is occasionally interrupted by transitions to southerly flow that have a limited offshore scale and appear to be manifestations of marine-layer flow that is rotationally trapped by the coastal mountains. Existing climatological and observational studies suggest that a synoptic-scale offshore flow initiates these coastally trapped disturbances (CTDs). Using idealized simulations produced with a 3D nonhydrostatic model, the authors find that an imposed offshore flow will produce CTDs in idealized coastal environments. The imposed flow first weakens the prevailing northerly flow in the marine layer and lowers the pressure at the coast. The marine-layer flow around this low pressure evolves toward geostrophic balance, but is retarded as it encounters the coastal mountains to the south of the low and subsequently deepens the marine layer in this region. The elevated marine layer then begins progressing northward as a Kelvin wave and later may steepen into a bore or gravity current, this progression being the CTD. Many observed features accompanying CTDs are found in the numerical simulations, including the formation of a mesoscale pressure trough offshore and deep southerlies in the CTD at the coast. Stability in the atmosphere above the marine layer can give rise to topographically trapped Rossby waves and stronger CTD winds. In these stable conditions, propagation of wave energy away from the disturbance does not preclude strong, quasi-steady, propagating CTDs.

1. Introduction

During the spring and summer, the climatological northerly flow along the U.S. west coast is occasionally interrupted by transitions to southerly flow that are often accompanied by low clouds, increased pressure, and colder temperatures (Bond et al. 1996). The transitions have a limited offshore scale and appear to be manifestations of marine-layer flow that is rotationally trapped by the coastal mountains; hence, they are commonly referred to as coastally trapped disturbances (CTDs). In a climatology of U.S. west coast CTDs, Mass and Bond (1996) find that CTDs are produced during specific larger-scale (synoptic scale) events characterized by the eastward movement of the climatological central-Pacific lower-tropospheric high into the Pacific Northwest, along with westward movement of the climatological southwestern U.S. low. In this paper we use numerical simulations to examine the linkage between this synoptic-scale evolution and the CTD-scale response, and the dynamics of the CTD.

Many CTD interpretations have been proposed in terms of Kelvin waves of various types (Gill 1977; Dorman 1985; Reason and Steyn 1992) or rotating gravity currents (Dorman 1987). These interpretations mainly concentrate on the character of the CTD and only indirectly address the synoptic-scale forcing. On the other hand, Mass and Albright (1987) view the CTD as a direct response of the marine layer to an along-coast synoptic-scale pressure gradient, and Mass and Bond (1996) argue that the along-coast pressure gradient (a coastal low) is produced by lee troughing associated with the synoptic-scale offshore flow (and also possibly by thermal troughing associated with the flow of heated air off the high desert). The connection between large-scale forcing and wave response is considered in the context of the linearized shallow water equations (SWE) by Rogerson and Samuelson (1995) who suggest that the imposition of a surface low at the coast, or the passage of a low across the coast, will produce propagating disturbances that resemble observed CTDs. Debate continues (Dorman 1997; Mass and Bond 1997), however, since the SWE do not provide a clear link between the synoptic-scale evolution (most often parameterized as an external pressure force in the SWE) and the CTD because of ambiguity in understanding the nature of the external forcing applied in the SWE. The SWE, by their nature, do not predict the evolution of the atmosphere outside the marine layer, nor do they

* The National Center for Atmospheric Research is sponsored by the National Science Foundation.

Corresponding author address: Dr. William C. Skamarock, NCAR, P.O. Box 3000, Boulder, CO 80307-3000.
E-mail: skamaroc@ncar.ucar.edu

© 1999 American Meteorological Society

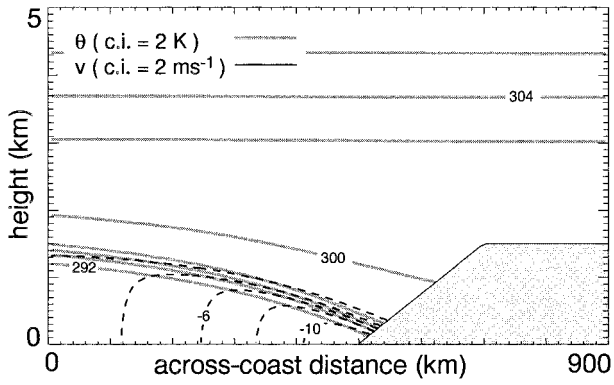

FIG. 1. Idealized climatological basic state and coastal topography. Negative contours are dashed.

include the dynamics associated with a finite-thickness marine inversion. Also, including a sloping side wall (characteristic of the actual topography) in the SWE is a nontrivial matter. Thus, we are motivated to numerically solve the 3D nonhydrostatic primitive equations in order to obtain a clearer picture of the linkage between the large-scale forcing and the CTD.

Based on the synoptic evolution outlined by Mass and Bond (1996), we have chosen to examine the effects of synoptic-scale easterly (across coast) flow through a region containing an idealized representation of the climatological mean state; a marine inversion with a balanced low-level northerly jet (along coast), along with an idealized coastal topography (Fig. 1). These simulations produce CTDs, and the CTDs exhibit Kelvin wave–like behavior in that they have a limited offshore extent and the along-coast velocity and pressure are generally in phase. Part of the difficulty in separating the Kelvin wave–like behavior from the larger-scale behavior lies in the role played by the atmosphere above the marine layer in CTD evolution. Many observed features accompanying CTDs, most notably deep southerlies along the coast and far-inland disturbances that also propagate northward, are obviously dependent on the dynamics of the atmosphere above the marine layer. These features are present in our simulated CTDs, and we have identified topographically trapped propagating Rossby waves in our simulations as being partly responsible for these features. Although the motions associated with the atmosphere above the marine layer can help explain some puzzling features of the observations, sensitivity tests removing the stratification aloft indicate that that the atmospheric structure above the marine layer is not essential for the production of a CTD.

2. Idealization and 2D dynamics

In a climatological study of the summer season marine environment over the eastern Pacific, Neiburger et al. (1961) found that a stable marine layer almost always exists off the California coast during the summer season (see their Fig. 20). At the coast, the climatological mean inversion intersects the coastal mountains where the inversion base is approximately 400 m above sea level and the inversion has a thickness of upward of 600 m. The marine layer deepens to the west of the coast with the inversion base rising to over 1500 m about 1000 km offshore. The inversion thickness remains approximately constant but the inversion strength weakens to the west (see Neiburger et al. 1961, Fig. 31). A geostrophically balanced along-coast jet accompanies this marine layer [Zemba and Friehe (1987); not shown in Neiburger et al. (1961)], with northerly winds achieving a maximum amplitude of approximately 10 m s^{-1} in the inversion at the coast.

Our idealization of this climatological mean state is depicted in Fig. 1, and an analytical description of the mean state and topography is given in the appendix. The idealized terrain in Fig. 1 represents the general rise from sea level to the Sierras and does not include any representation of the coastal range. The inversion is modeled after the climatology of Neiburger et al. (1961), although we do not weaken the inversion to the west as in the climatology. Contrary to observations (Zemba and Friehe 1987), our northerly jet is constant with height in the marine layer because we do not include the complicating effects of surface drag and surface heat fluxes. The mean potential temperature profile above the marine layer is less stable below 2500 m and reflects observations (Ralph et al. 1998) showing the atmosphere to be more weakly stratified in a 1–2 km thick layer above the marine inversion preceding and during many CTD events.

In Mass and Bond's (1996) climatology of CTDs, those events occurring along the California coast are well illustrated by the climatology associated with transitions (wind reversals) measured at buoy 13 located approximately 100 km northwest of San Francisco. Most striking in the CTD climatology is the offshore flow at 850 mb (Mass and Bond 1996, Fig. 7) preceding and during CTD events that does not exist in the mean climatology (Mass and Bond 1996, Fig. 1). The CTD climatology shows that this offshore flow is largely geostrophically balanced and results from the eastward movement of the Pacific high into the Pacific Northwest along with the westward movement of the southwestern U.S. low.

Given the robustness of this large-scale signal (the offshore flow) we are motivated to examine the effects of an easterly wind blowing offshore in an idealized environment. To this end, we have performed simulations integrating the nonhydrostatic compressible equations using a model similar to that described in Durran and Klemp (1983), but with the addition of a semi-Lagrangian monotonic integration scheme for the potential temperature θ. The semi-Lagrangian scheme uses the tensor product of 1D Hermite polynomials with the cubic derivative estimate for interpolations as described in Williamson and Rasch (1989), and the interpolators

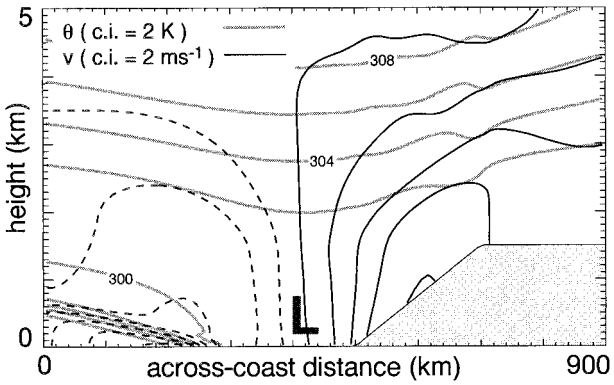

FIG. 2. Potential temperature and along-coast velocity (contoured as in Fig. 1) for the 2D simulation at day 1.5 with the imposed offshore flow using the topography and basic state in Fig. 1. Negative contours are dashed and L denotes the minimum pressure in the lee trough.

are monotinized using their condition [(2.19)]. The monotonic scheme for θ is needed in order to maintain the sharp marine inversion without explicit numerical filtering (which would remove the marine layer and inversion over time); the centered-in-space-and-time leapfrog scheme requires excessive numerical filtering to remove noise generated at the inversion and CTD edges. Using the monotonic semi-Lagrangian scheme, we have removed all explicit numerical filters and dissipation in the θ equation, and we use only a horizontal fourth-order filter in the momentum equations.

In the 2D simulations, the imposed easterly wind has the form $U = U_0 \sin^2(\pi t/T)$ and is uniform in x (the across-coast direction) and z with $U_0 = -6$ m s^{-1} and $T = 3$ days. This easterly flow is assumed to be balanced by a north–south pressure gradient that is also imposed in the model; hence, the imposition of this flow does not engender any geostrophic adjustment in and of itself. In this regard, we are assuming a quasigeostrophic balance for the imposed large-scale flow; the geostrophic adjustment of the flow to the imposed pressure gradient (the large-scale forcing) is assumed to be instantaneous. The balanced easterlies in this flow field are not accompanied by a north–south temperature gradient because the easterlies are constant with height.

Figure 2 depicts results from a 2D (x, z) simulation where this barotropic easterly flow is imposed over the terrain depicted in Fig. 1. The marine layer and northerly jet are advected offshore away from the plateau, the northerly jet intensifies offshore (increasing from 10 to over 14 m s^{-1}), and a deep layer of southerlies forms above the plateau. This two-dimensional evolution has some similarities to a CTD event: formation of a low at the coast, movement offshore and intensification of the northerly jet, and southerlies forming at the coast. The coastal southerlies are not the CTD since they are not accompanied by a rising marine layer and higher pressure. However, the lee trough and vortex may partially explain the often observed deep southerlies and

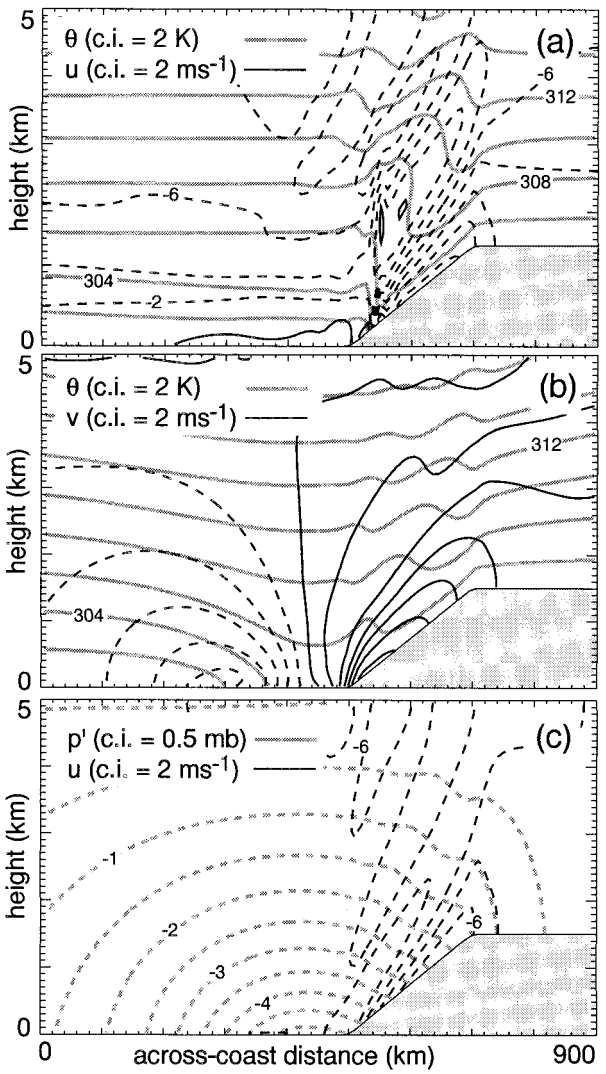

FIG. 3. (a) Potential temperature and across-coast velocity for the 2D simulation with constant atmospheric stability ($N = 10^{-2}$ s^{-1}) and no rotation ($f = 0$) at 1.5 days. (b) The same simulation with rotation included ($f = 10^{-4}$ s^{-1}); potential temperature and along-coast velocity are contoured. (c) Perturbation pressure and across-coast velocity for the simulation with rotation. Negative contours are dashed.

the movement offshore and intensification of the northerly jet.

The earth's rotation plays a crucial role in allowing the marine layer (or any stably stratified layer) to be the pushed away from the coastal plateau by an offshore flow. The importance of earth's rotation is illustrated in results from two simulations of flow down a plateau in an atmosphere with constant stability $N = 10^{-2}$ s^{-1}, without and with earth's rotation, given in Fig. 3. There is no marine layer in these simulations, and the Coriolis parameter $f = 0$ in the first simulation and $f = 10^{-4}$ s^{-1} in the second. Figure 3a shows the potential temperature and across-coast wind at day 1.5 (the time of the maximum imposed easterly wind) for the simulation

without background rotation ($f = 0$); in this case the fluid layer below the plateau is not evacuated by the easterly flow. A highly nonlinear hydraulic-jump-like feature is evident above the plateau slope (note the vertical isotherms), and flow reversal has occurred at its base. Figures 3b and 3c show the potential temperature, pressure, u, and v fields for the second case where $f = 10^{-4}$ s^{-1}; cyclonic flow has developed on the plateau and the fluid layer below the plateau is evacuated. The pressure has lowered on the plateau and a lee trough and vortex have formed.

Following Pierrehumbert (1984), one can estimate that, in the case without earth's rotation, $|u'|/U_0 \sim NH_0/U_0$ ($= 2.5$ here), where N is the mean stability, H_0 the height of the plateau, and U_0 the imposed wind speed. Therefore, the flow is expected to be highly nonlinear. What is less obvious is the dynamical evolution that leads to flow blockage. The simplest explanation is that the buoyancy force resulting from bringing warm air down the slope becomes stronger than the inertia associated with the downslope wind (the Froude number NH_0/U_0 is a measure of the ratio of these two forces), and this results in the separation and stagnation seen in the lower layers in Fig. 3a. In the case with earth's rotation, one can estimate that $|u'|/U_0 \sim NH_0/fL_{\text{pl}} \ll 1$, where L_{pl} is the plateau horizontal length scale. The dynamics is essentially linear, and the cold air is moved away from the plateau. Physically, the buoyancy force is balanced by the developing cyclonic rotation and does not engender separation, and the inertia of the downslope wind can move the cold air away.

As expected from these scalings in the case with earth's rotation, increasing (decreasing) the mean stratification or the plateau height would increase (decrease) the amplitude of the lee trough and along-coast wind fields in these idealizations. Numerical tests confirm these relationships.

3. CTD simulations in idealized environments

a. Reference case

Using the idealized climatology in Fig. 1, we impose the easterly flow over a finite-length along-coast region in the 3D simulation. The imposed flow has a limited along-coast extent in the 3D realization and has the functional form

$$U = U_0 \sin^2\left(\pi\frac{t}{T}\right)\cos^2\left(\pi\frac{y - y_c}{L_e}\right), \quad \text{for } \frac{|y - y_c|}{L_e} < \frac{1}{2}.$$

As in the 2D simulations, we use $U_0 = 6$ m s^{-1} and $T = 3$ days, but now include an along-coast jet width $L_e = 600$ km. The simulation domain has an along-coast length of 1800 km, an across-coast length of 900 km, and the finite-difference grid lengths are $\Delta x = \Delta y = 20$ km. Open boundary conditions of the form used in Klemp and Wilhelmson (1978) are imposed at all lateral boundaries and a radiation condition described in Durran (1995) is used at the upper boundary located at $z = 5$ km. The domain is large horizontally so as to minimize lateral boundary effects. Although the domain is rather shallow, we have conducted tests with deeper domains and found little difference in the solutions.

Figure 4 shows horizontal cross sections of the horizontal wind vectors and potential temperature at 300 m above the sea surface for every 12 h from 1 to 2.5 days. By day 1 there is a noticeable depression in the marine layer centered slightly south of the offshore-jet maximum, with a slight acceleration of the northerly jet to the west of this depression. The southward movement of the depression is caused by the northerly jet; simulations with no jet (a flat marine inversion) do not show any significant southward movement of the depression. Also at this time there is a weak onshore-flow component to the south of the depression. The potential temperature is a reasonable surrogate for the perturbation pressure field at this level, and while initially there is flow down the pressure gradient into the depression, the flow quickly adjusts toward a geostrophic balance with cyclonic flow around the depression.

The marine layer continues to deepen to the south of the depression over the next 1/2 day, and by day 1.5 this elevated region has begun to propagate to the north and has reached the center of the imposed offshore jet. The surge continues to propagate to the north through the next day, and the marine layer continues to deepen to the south of the offshore jet. As the CTD propagates to the north it cuts off part of the marine-layer depression offshore, creating a closed mesoscale low away from the coast. This low slowly moves to the south. Later in the integration the CTD continues to propagate northward into the region where the northerly jet has not migrated offshore, and the CTD decays (not shown).

Horizontal cross sections of full pressure and velocity vectors at 20 m above the sea surface for days 0, 1, and 2 are shown in Fig. 5. The pressure gradient balancing the northerly marine layer jet is obvious at day 0, and the north–south high–low pressure gradient balancing the imposed offshore flow can be discerned at day 1. Weak onshore flow to the south of the coastal low is beginning to form at day 1. By day 2 the onshore flow to the south of the low is substantial, and the CTD has formed and is propagating to the north, creating a closed mesoscale low located well to the south of the leading edge of the CTD. The flow is largely geostrophic at this time except in the vicinity of the leading edge of the CTD and in the coastal region to the south of the cutoff low.

An across-coast cross section at day 2.5, displayed in Fig. 6b, shows the marine layer piled against the coast to the south of the offshore jet, with a northerly jet maximum off the coast, a southerly jet maximum (the CTD) at the coast, and the low isolated offshore between the two jets. There exists southerly flow above the marine layer to the east of the low (in the coastal region), but this flow is weak as are the pressure perturbations

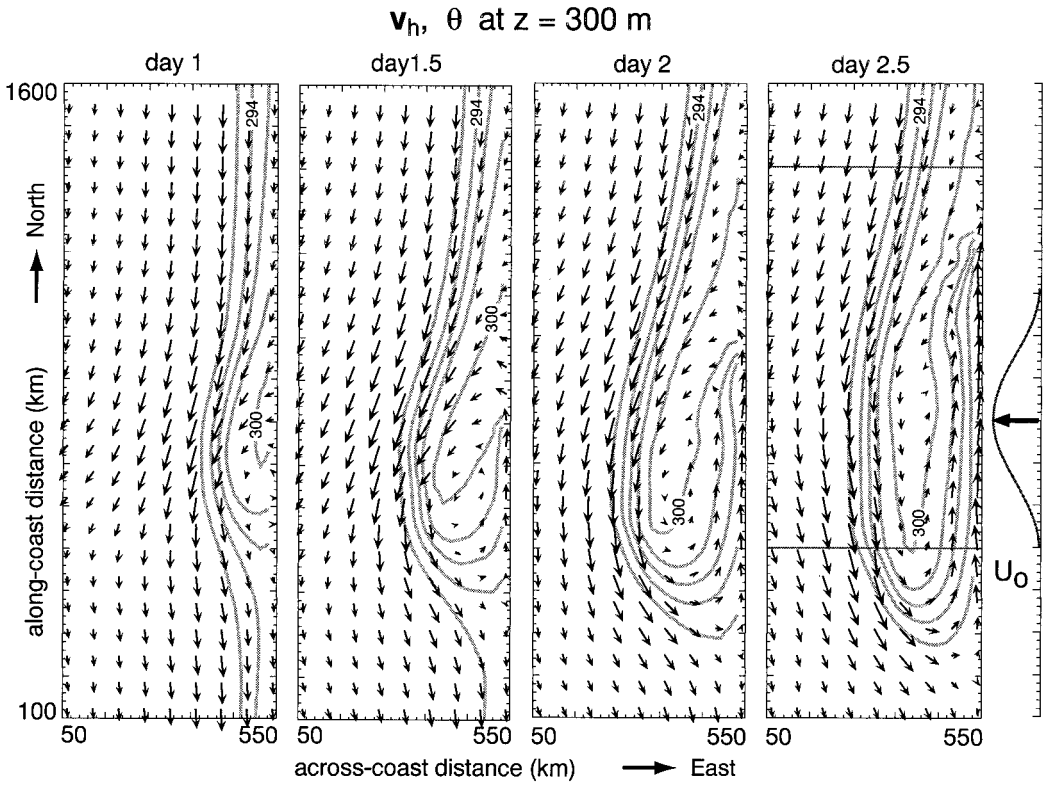

FIG. 4. Horizontal cross sections at $z = 300$ m from the reference simulation. Potential temperature is contoured in gray (contour interval, c.i., = 2 K). Maximum vectors are approximately 14 m s^{-1}. The coastal mountains intersect the plane at $x = 540$ km. The position of the imposed jet is indicated on the far right and the horizontal lines at day 2.5 denote the positions of the vertical cross sections in Fig. 6.

associated with it. To the north of the imposed offshore flow and CTD (Fig. 6a), the marine layer and northerly jet have not moved significantly offshore.

Along-coast cross sections at days 1 and 2 are shown in Fig. 7. The onshore flow to the south of the imposed offshore flow has begun by day 1 (see Fig. 4), and although the southerlies (and CTD) have yet to appear, a gradual transition in along-coast velocity is beginning to form. The marine layer is deepening along the coast to the south of the imposed offshore flow, and the local alongshore pressure gradient weakens the prevailing northerly flow. This is the beginning of the CTD. By day 2 the CTD is well developed. A long region of southerly winds and elevated marine layer extends from the south, where there is a region of onshore flow induced by the coastal mesolow (not shown), north to the sharp leading edge of the CTD. Deep southerlies are also evident. The marine-layer depth is roughly constant, as is the along-coast velocity along most of the CTD. The marine layer is deepest to the south of the coastal mesolow and imposed offshore low. This region of deepest marine layer does not propagate with the CTD but rather is tied to the location of the coastal mesolow.

The imposed offshore flow has a significant effect on the atmosphere above the marine layer in the reference simulation. A northward-propagating disturbance above the marine layer can be detected in the along-coast cross sections in Fig. 7. The warming aloft (above the marine layer, coincident with a pressure minimum) is moving to the north over time as is its northern extent. This disturbance appears to be a topographically trapped Rossby wave and, in cases with strong atmospheric stratification above the marine layer, this wave can significantly alter the CTD and marine-layer response to the imposed offshore flow. The dynamics of, and interaction between, the CTD and trapped Rossby mode is discussed in section 4b. Stratification above the marine layer also increases the strength of the coastal low and can lead to increased along-coast southerlies along sections of the coast. This is discussed in more detail in section 4a.

b. Comparison with observations

The reference simulation, where the atmospheric evolution is forced by our idealization of the offshore flow observed in the CTD climatology (Mass and Bond 1996) reproduces many features observed in CTD events.

The offshore winds lead to the formation of a mesoscale low pressure anomaly at the coast, as observed in many cases, including the 10–11 June 1994 CTD

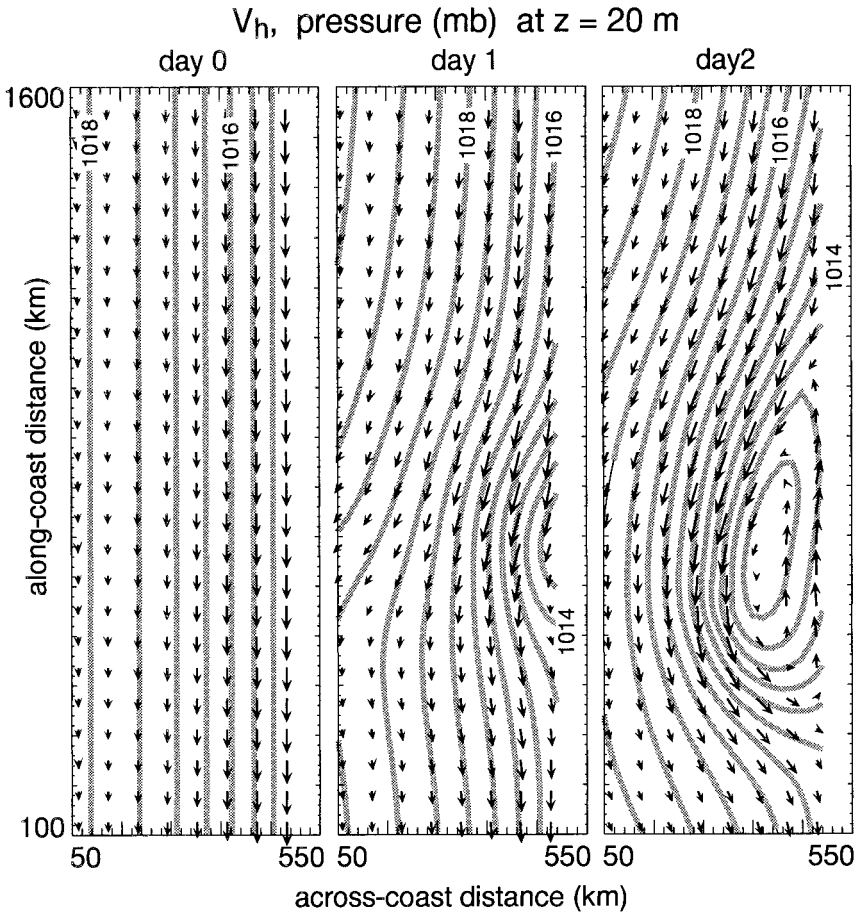

FIG. 5. Horizontal cross sections depicting the full pressure and velocity vectors at $z = 20$ m from the reference simulation. Pressure is contoured in gray (c.i. = 0.5 mb), and the maximum vectors are approximately 16 m s^{-1}. The plotting domain is the same as in Fig. 4.

(Ralph et al. 1998). The lowering of pressure is associated with warming aloft and depression (evacuation) of the marine layer, a process documented in the 10 June 1994 case by Ralph et al. (see their summary, Fig. 26). The rise in the marine layer to the south of the coastal low is observed in many cases, including the 10 June 1994 case, the 4–5 May 1982 and 5–7 June 1981 cases (Dorman 1985), the 15–17 May 1985 CTD (Mass and Albright 1987), and others.

The sharp leading edge of the CTD in the reference simulation is a feature that is often observed, particularly later in CTD events. A climatology by Bond et al. (1996) shows that the leading edge of CTDs are generally more abrupt at northern locations than at southern locations, suggesting that abrupt transitions develop with time as expected from nonlinear wave steepening (Reason and Steyn 1992). This evolution also occurs in our simulations, although the period during which the wave steepens into a discontinuity is short and a gravity-current or borelike character of the leading edge appears soon after the wave begins propagating. The passage of the leading edge is also accompanied by surface-pressure rises and wind shifts (as observed) and surface-temperature falls (sometimes observed).

The temporal and spatial scales of the simulated CTD generally coincide with observed CTDs. The recognizable coastal low forms within a day and a propagating CTD appears within a half-day after that. Propagation speeds for the reference case CTD, and in other simulations to be presented, are on the order of 5–10 m s^{-1}, a range of values that bracket the observations. The offshore extent of the southerlies is of order 100 km, comparable to the Rossby radius ($R = \sqrt{g'h}/f$, where h is the marine layer height), and the alongshore extent of the southerlies can extend many hundreds to over a thousand kilometers at later times in the CTD life cycle. These length scales are generally consistent with observations.

The evolution of many features apart from the CTD itself is also captured in the reference simulation. The coastal low gradually elongates (in the along-coast direction) as its center moves offshore. This pattern has been observed in many cases, including the 10 June 1994 case (Ralph et al. 1998) where ship data document

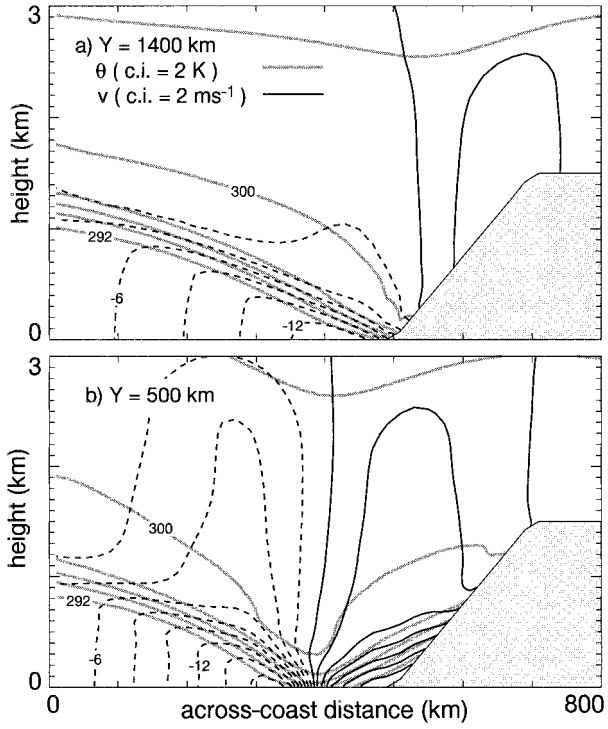

FIG. 6. Across-coast vertical cross sections at day 2.5 for the reference simulation. Negative contours are dashed and cross-section locations are indicated in Fig. 4.

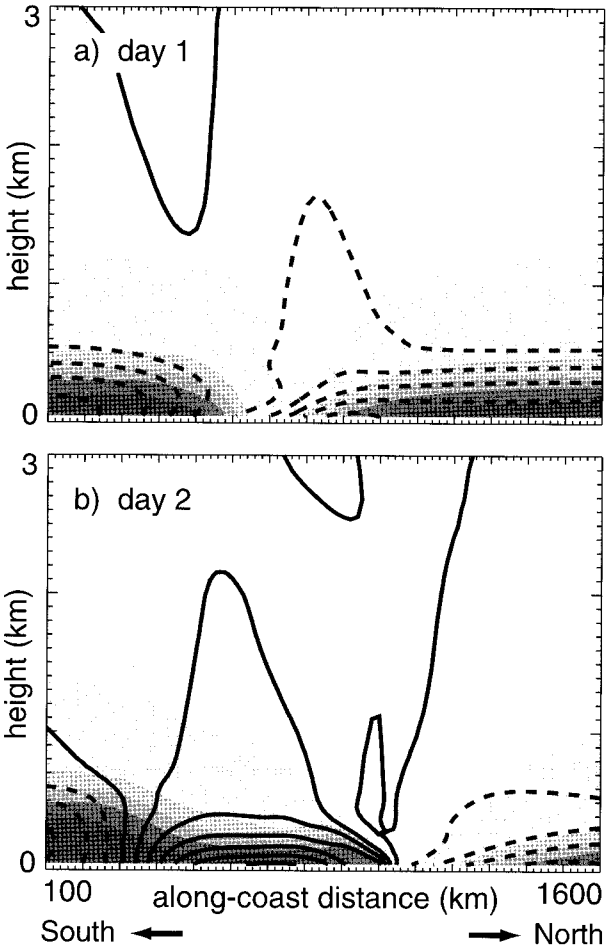

FIG. 7. Along-coast vertical cross sections at $x = 500$ km (the base of the plateau), where potential temperature is shaded with c.i. = 2 K and along-coast velocity is contoured with c.i. = 2 m s^{-1}. Negative contours are dashed.

the offshore pressure minimum in the latter stages of the CTD event. Southerlies above the marine layer at the coast, observed in the 10 June 1994 case, are also found in the reference simulation. Intensification and offshore migration of the northerly jet at early times in the CTD event prior to CTD passage also occur in both observed cases and the reference simulation.

Mass and Albright (1987, 1988) observe propagating pressure signals far inland from the coast that appear to be in phase with the CTD (at Sacramento, California, and Reno, Nevada, for the 3–5 May 1982 case). We see pressure changes inland in our reference simulation that appear similar to the inland signal observed by Mass and Albright. They also show that pressure changes at the coast in the 3–5 May 1982 case cannot be accounted for solely by changes in the marine-layer elevation. The surface pressure changes in the reference simulation (at the coast) are largely due to changes in marine-layer elevation. We have, however, found that the magnitude of the surface pressure signals associated with atmospheric dynamics outside the marine layer, both at the coast and inland, depend critically on the overall elevation rise of the mountains and atmospheric stability. The climatological mean state has only weak stability above the marine layer (Neiburger et al. 1961); thus large surface pressure signals (both in the marine layer and inland), resulting from free-atmosphere dynamics, can only be created by significantly increasing the atmospheric stability above the marine layer. Numerical tests confirm this hypothesis.

Our simulation also reproduces many features found in the Thompson et al. (1997) simulation of the 10–11 June 1994 CTD. Their simulated event produced a coastal low through lee troughing (as demonstrated using parallel simulations with and without coastal topography), and this leads to onshore flow to the south of the coastal low [see Figs. 4, 6, 10, and 23 in Thompson et al. (1997)], followed by the CTD. Their CTD possessed the character of a gravity current, identified as such by its sharp leading edge density gradient, and the deeper marine boundary layer to the south of the leading edge. Both of these features are captured in our CTD simulation (see Fig. 7).

4. Propagating modes

a. Kelvin wave and gravity current dynamics

In simulations that include a marine layer, the CTD itself begins with a deepening of the marine layer to the

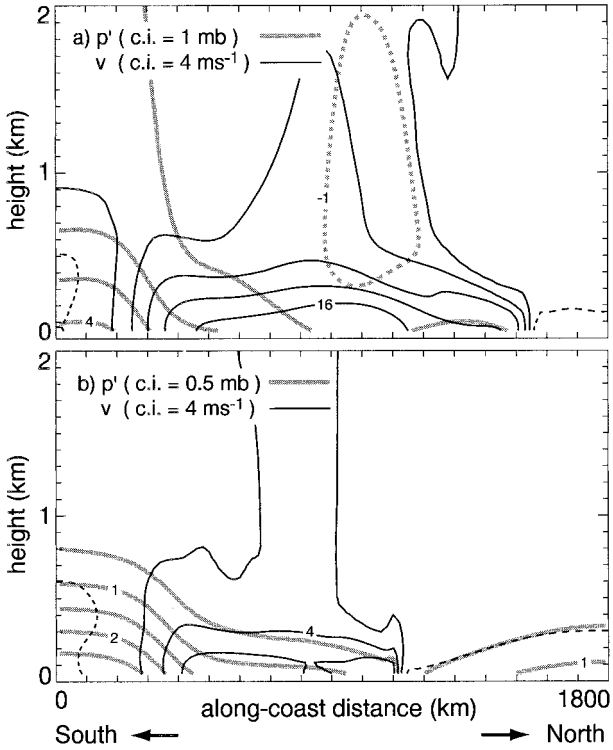

FIG. 8. Along-coast vertical cross sections at $x = 500$ km at day 3 for (a) the reference case and (b) the neutral case. Negative contours are dashed.

south of the coastal mesoscale low pressure; this deepening is produced as onshore (westerly) flow, associated with the mesoscale low, encounters the coast. At early times the CTD waveform is smooth as the disturbance propagates along the coast to the north. The CTDs in these simulations quickly steepen at their leading edge where nonlinear effects are strong because the CTD height is much greater than the marine-layer height into which it is propagating; indeed, the marine layer is almost completely evacuated from the coast by the offshore flow ahead of the CTDs.

In observational studies, much emphasis has been placed on classifying CTDs as waves or gravity currents or bores. Our view is that the disturbances are all Kelvin wave–like in the sense that the pressure and along-coast velocity decay exponentially with distance from the coast (as indicated by the velocity vectors in Fig. 4 at 2 and 2.5 days, and from θ, pressure, and along-coast velocity v in Fig. 6b), and that the pressure and along-coast velocity are generally in phase. Figure 8 depicts along-coast cross sections of pressure and along-coast velocity for the reference simulation and for a simulation wherein the atmosphere above the marine layer has neutral stability. The region of the relatively uniform strong southerlies in the neutral case (Fig. 8b), extending from 400 to 1100 km, is accompanied by nearly uniform high pressure. The nose of the gravity current is at the north edge of this zone. Higher pressure and an elevated marine layer, caused by the onshore flow, are found to the south of this zone, and the strong along-coast pressure gradient in the region of accelerating southerlies (from 200 to 400 km) is consistent with the initiation of the Kelvin wave by localized deepening of the marine layer near the coast. This source region does not propagate with the CTD; rather it is tied to the location of the offshore mesoscale low.

The phase relation between the along-coast velocity and pressure is somewhat modified by the presence of stability above the marine layer (Fig. 8a). The along-coast pressure is not uniformly high in the region of the southerlies. In a 300-km length region to the south of the leading edge (from 1200 to 1500 km) relatively uniform high pressure is coincident with constant alongshore velocity. The strong along-coast pressure gradient and region of accelerating southerlies associated with the raised marine layer in the southern region (from 200 to 500 km) is similar to that in the neutral atmosphere case (Fig. 8b), and as in the neutral case this region of elevated marine layer does not propagate with the CTD. Between these regions lie somewhat stronger along-coast winds associated with a pressure minimum (from 800 to 1200 km). Here the alongshore southerlies are augmented by southerly flow promoted by the offshore low. These southerlies extend well above the marine layer. To reiterate, the CTD itself is Kelvin wave–like; it decays away from the coast and the along-coast velocity and pressure are generally in phase. However, the offshore low can modify this signature at times in various places.

Typically, Kelvin wave and bore models are formulated within a shallow water equations framework that, within the atmosphere, corresponds to a dense layer of fluid with a less dense, unbounded, neutral atmosphere above. These models predict constant propagation speeds for disturbances in vertically unbounded neutral atmospheres, with energy conserved in the Kelvin wave solutions and dissipated in the bore solutions. In stratified atmospheres, however, we expect wave decay through energy loss from vertically propagating gravity waves as indicated in the linear solutions of Rhines (1970) depicting Kelvin waves that propagate vertically as well as horizontally.

In order to examine this question of wave and gravity-current decay, we consider the simpler case of disturbances generated by a ''dam break'' starting from a semi-infinite reservoir with an overlying stratified or neutral atmosphere within a rotating reference frame. The dense fluid behind the dam is specified as a cold perturbation decreasing linearly from 0 K at $z = 2$ km to -5.0 K at the surface superposed over an atmosphere possessing constant stratification $N = 10^{-2}$ s^{-1} in the stratified case and $N = 0$ in the neutral case. A free-slip wall, representing the coastal mountains, is located perpendicular to the dam on the east (right) boundary of the domain.

Figure 9 shows horizontal cross sections for the strat-

ified and neutral environments, and vertical cross sections at the wall for these cases are given in Fig. 10. In both cases CTD-like responses are obtained that maintain amplitude and structure while lengthening over time. The disturbances are strongly nonlinear, suggesting a gravity-current-like character evidenced by the near discontinuity at the leading edge at the surface. In the stratified-atmosphere case, however, the turbulent dissipation typically existing in the head of the gravity current or bore is replaced by energy loss through vertically radiating gravity waves. Steady currents are produced with this radiative energy loss. Thus, stratification in a vertically unbounded atmosphere does not preclude the existence of strong propagating CTDs, but in environments with significant stratification the perturbations must be strong enough to produce discontinuities at the leading edge if they are to produce CTD-like disturbances. If the initial perturbations are weak, simulations (not shown) indicate that CTD-like disturbances are not produced.

b. CTD dynamics and topographically trapped Rossby waves

Two simulations were performed to examine the effect of the topographically trapped Rossby wave on CTD evolution, one having a neutral atmosphere on which the marine layer is superposed (the *neutral* case, within which the Rossby wave is absent) and the other having constant stability atmosphere $N = 10^{-2}$ s^{-1} accompanying the marine layer (the *stratified* case, within which a Rossby wave is present). The solutions, displayed in Fig. 11, evolve similarly to and bracket the reference simulation described in section 3. They also demonstrate that stratification above the marine layer can significantly alter CTD evolution. Most notably, the marine layer and northerly jet are displaced farther west (away from the coast) in the neutral case compared with the stratified case and the CTD propagates at a higher speed in the stratified case.

The topographically trapped propagating Rossby wave can be observed in horizontal cross sections of perturbation pressure at $z = 1.8$ km in the stratified simulation, shown in Fig. 12. The the central low pressure in the wave does not propagate very far over the three days because it is sustained by the forcing (imposed offshore flow) that is applied at a fixed location. The northern boundary of the wave propagates rapidly, and the wave propagation coupled with the fixed forcing result in the elongated appearance of the wave.

The propagation mechanism for the Rossby wave is illustrated schematically in Fig. 13. The balanced flow associated with the low (high) pressure produces downslope (upslope) flow to its north. The stratification leads to warming (cooling) and hydrostatic pressure falls (rises) in the downslope (upslope) flow region, and hence northward propagation of the pattern.

Rhines (1970) developed a linear model for a Rossby wave for a constant-stratification atmosphere with a constant-slope bottom boundary. The propagating upper-level waves found in our simulations exhibit vertical decay and horizontal phase speeds consistent with those suggested by Rhines' theory, which predicts exponential decay with height ($e^{-\mu z}$) where the decay scale $\mu = (N/f)(k^2 + l^2)^{1/2}$ (k and l are the across- and along-slope wavenumbers, respectively). Using values from the stratified simulation, $N = 10^{-2}$ s^{-1}, $f = 10^{-4}$ s^{-1}, and a nominal wavelength of $L_x = L_y \sim 600$ km, yields $\mu \simeq 10^{-3}$ m^{-1}, a decay-scale height of approximately a kilometer. The vertical extent of the topographically trapped Rossby wave in these simulations is shallow (a few kilometers). This is illustrated in the vertical decay of low pressure above the marine layer observed in the vertical cross section from the reference simulation (Fig. 8a). The along-coast phase speed of the linear wave from Rhines theory, using the parameters from the stratified simulation, is approximately 7 m s^{-1}. As can be seen in Figs. 7 and 8, the northern extent of the upper-level wave propagates to the north with a nominal speed on the order of 10 m s^{-1}.

The Rossby wave exists because the atmosphere is

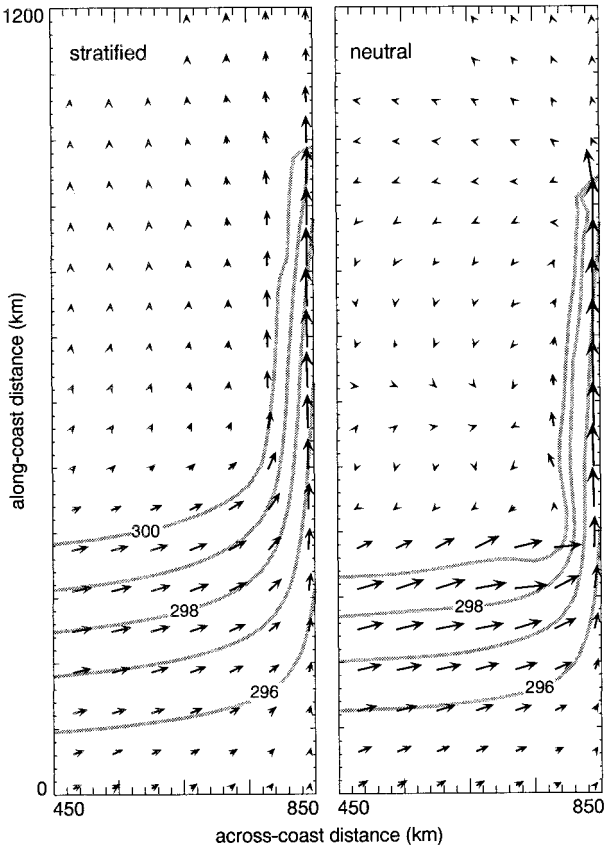

FIG. 9. Horizontal cross sections at $z = 100$ m for the dam break simulations. The dam is located at $x = 32$ km. Potential temperature is contoured in gray with c.i. = 1 K, and the maximum velocity vectors are 10.7 and 13.0 m s^{-1} in the stratified and neutral cases, respectively. A free-slip vertical wall is located at $x = 850$ km.

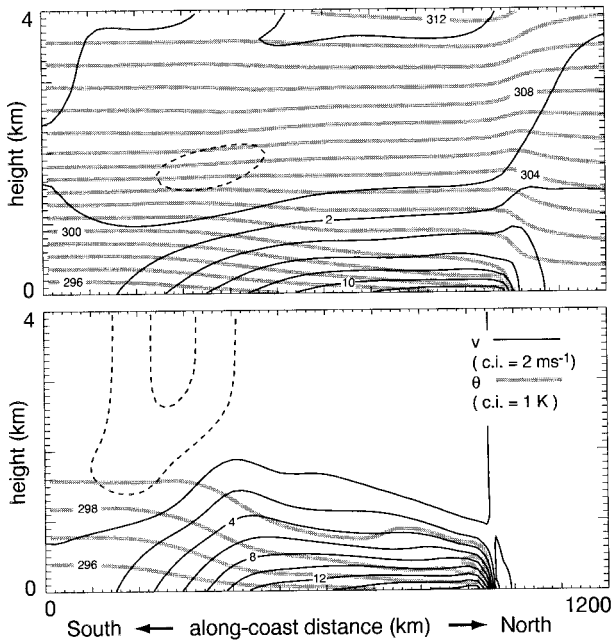

FIG. 10. Along-coast vertical cross sections at $x = 850$ km for the dam break simulations for the stratified (top) and neutral (bottom) cases. Negative contours are dashed.

stratified above the marine layer, and the wave modifies the marine-layer disturbance that we call the CTD. We have also found, however, that CTD-like disturbances can be produced in simulations that do not contain a marine layer. In a simulation using the terrain in Fig. 1 and an atmosphere with constant stratification but no marine layer, a propagating disturbance similar to a CTD is produced when the imposed offshore flow is sufficiently strong. This evolution is depicted in Fig. 14 for $U_0 = 6$ m s^{-1}. While part of the disturbance can be characterized as a topographically trapped Rossby wave, warm air advected off the coast eventually induces flow up the slope that is blocked. The blocked flow produces a mound of cold air, much as in the case with the marine layer, and a CTD-like propagating disturbance is produced. The CTD is characterized by rising pressure and falling temperatures at its leading edge and propagates to the north at 6.5 m s^{-1}. Strong southerlies are found along the coast and northerlies are found away from the coast. A lee trough (mesoscale coastal low) is also produced, although the absence of the sloping marine layer and accompanying northerly jet reduces the along-coast extent of the low (the northerly jet advects the warm air to the south). As in the other stratified cases, the offshore extent of the CTD and coastal low is less than that found in the simulations with reduced stratification. Nonlinearity in the resulting wave motion is found to be crucial in producing a CTD-like disturbance. If the imposed offshore flow is weak, only a Rossby mode is produced; coastal southerlies and a trough extending offshore do not appear.

The Rossby wave appears primarily responsible for the differences between the neutral and stratified simulations containing a marine layer (depicted in Fig. 11). With respect to the offshore displacement of the marine layer (and the scale of the associated offshore low pressure), the upper-level Rossby wave in the stratified case, being itself displaced to the north, produces a balanced wind field that opposes the imposed offshore flow. This opposition reduces the offshore displacement of the marine layer and northerly jet compared with that in the neutral case (which lacks this upper-level wave). We find that a stronger offshore wind is generally needed to produce a CTD-like response with increasing stratification above the marine layer. The northward displacement of the coastal low in the stratified case relative to that in the neutral case is also in part attributable to the upper-level Rossby wave. The faster northern progression of the CTD in the stratified case as compared to the neutral case is due to the stronger mesoscale low pressure that forms when stratification is present above the marine layer. The stronger low pressure leads to a more pronounced onshore flow to the south of the low and to faster CTD propagation and to stronger along-coast winds in the CTD (cf. Figs. 8a and 8b, and the neutral and stratified cases in Fig. 11).

The onshore flow associated with the early lee trough is located over 500 km to the south of the centerline of the imposed offshore jet in both the stratified and neutral simulations shown in Fig. 11, and this region of onshore flow does not propagate to the north. Figure 11 also shows that, in the stratified case, a second region of onshore flow is propagating to the north; this region is just to the south of the centerline of the imposed offshore jet at day 2.5. This propagating onshore flow is driven by the propagating Rossby wave, and accelerates the southerlies locally. In the stratified case (Fig. 11), the leading edge of the CTD is over 500 km to the north of this region of onshore flow and propagating away from it. However, if the Rossby wave propagation speed is equal to or greater than the propagation speed of the CTD forced by the offshore flow, then it is possible that the Rossby wave would be the dominant signal in the CTD event. In this case the CTD would be tied to a coastal low pressure feature that propagates up the coast. The CTD would no longer be freely propagating, but would be continually regenerated by the northward-progressing onshore flow.

In observed CTD events, Mass and Albright (1987) identify a coastal low and along-coast pressure gradients that propagate with the CTDs. They argue that these features are part of the synoptic evolution, and that the CTD is a direct response to the propagating along-coast pressure gradient (southerly accelerations along the coast into the low). We believe that propagating Rossby waves are likely responsible for the propagating coastal lows and propagating along-coast mesoscale pressure gradients in observed CTD events, and thus, that they are a response to the synoptic forcing and not the syn-

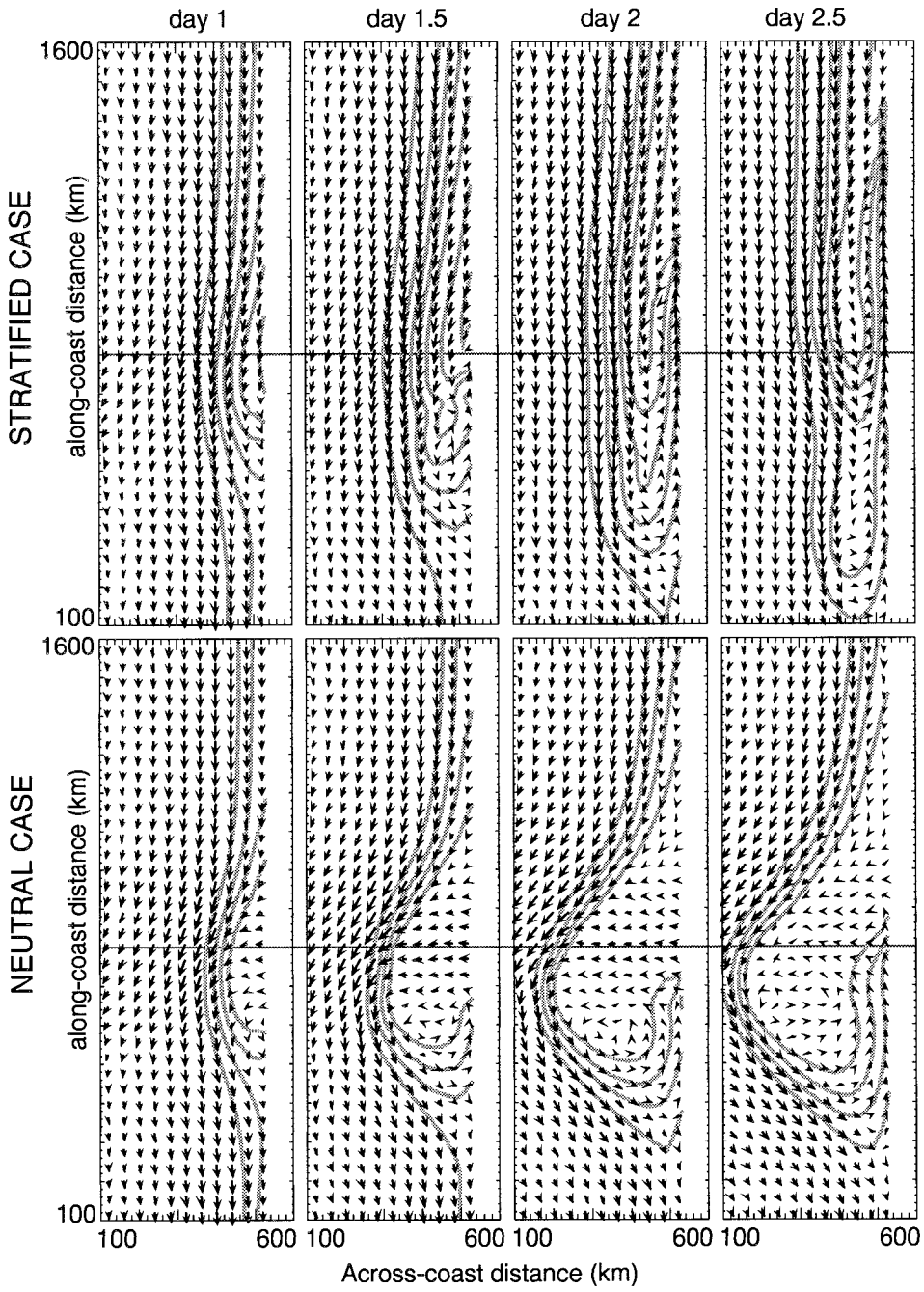

FIG. 11. Horizontal cross sections at $z = 300$ m of potential temperature (gray, c.i. = 2 K) and velocity vectors for the neutral and stratified simulations. The thin line is the centerline of the imposed offshore flow.

optic forcing itself. The synoptic forcing is characterized by offshore flow and a positive pressure gradient directed to the north. The evidence presented here indicates that the production of a CTD from an alongshore pressure gradient is an indirect response to the coastal low, which itself is a response to a synoptic-scale north–south high–low pressure field. The primary effect of the coastal low is to produce flow into the coast to its south that raises the marine layer at the coast, and it is the locally elevated marine layer that initiates southerly flow and a CTD.

c. Terrain

The idealized topography in Fig. 1 has a shallower slope (1.5 km/200 km) than the average slope of the

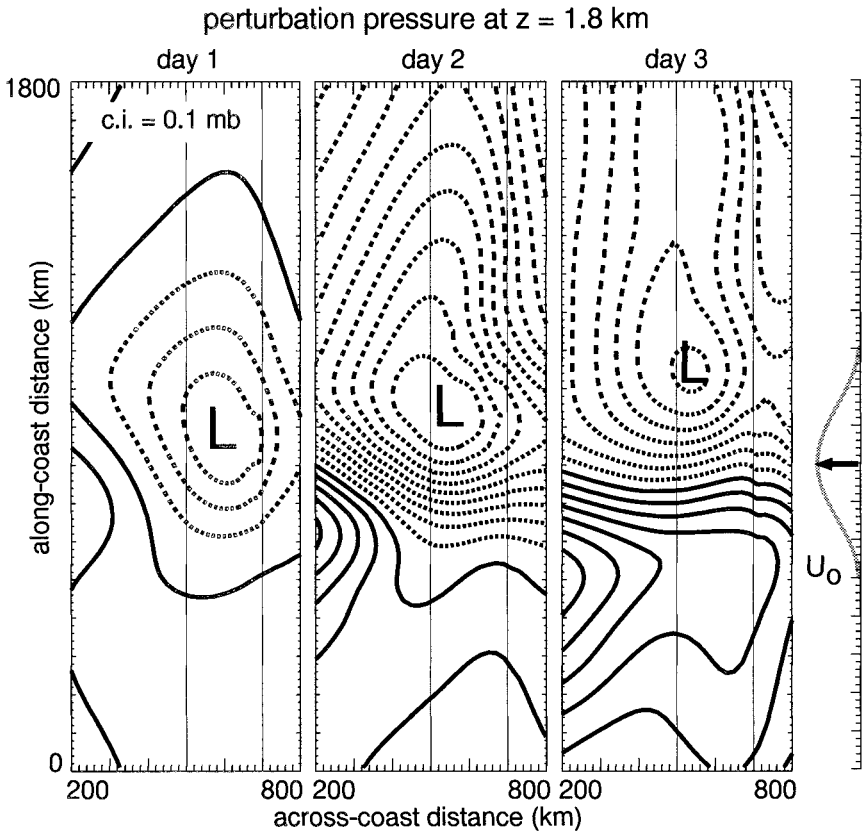

FIG. 12. Horizontal cross sections, of perturbation pressure at 1.8 km for the stratified case. The bottom and top of the plateau are denoted by the thin lines at $x = 500$ km and $x = 700$ km. Negative contours are dashed.

coastal mountain range in California (closer to 1 km/50 km) and a much simpler shape than the Californian topography (a coastal range followed by a valley and then the Sierras). We have performed simulations similar to our reference simulations using the somewhat more realistic topography depicted in Fig. 15 (the shape of the topography is described in the appendix). The CTD evolution in a simulation using the more realistic topography (and 10-km horizontal resolution) and the same reference sounding, marine layer, and imposed offshore flow as in the reference simulation is given in Fig. 16 and can be compared with the reference simulation (Fig. 4). A more pronounced isolated offshore low is present in this simulation, the offshore extent of the CTD is smaller, and the CTD leading edge is a little farther to the north after 2.5 days. All of these effects are associated with the steeper slope of the more realistic topography at the coast, and with the larger elevation change and mean slope between the coast and the crest of the Sierras (the plateau has a height of 1.5 km in the topography of Fig. 1 and 2 km in the more realistic topography). The higher plateau leads to a stronger lee vortex and the greater slope leads to higher propagation speeds for the topographically trapped Rossby waves. In general the fundamental dynamics is the same in both cases; the role of the mountains is to block low-level westerly flow in the marine layer and, when the atmospheric stratification is sufficient, to promote lee troughing and topographically trapped Rossby wave propagation.

d. Potential vorticity

Based on observations and mesoscale model simulations of the 10 June 1994 CTD event, Persson et al. (1995) have proposed that the along-coast flow reversal of the CTD (winds evolving from northerlies to southerlies) is driven by the circulation induced by a positive potential vorticity (PV) plume, and that the PV plume is generated through differential frictional effects as the synoptic-scale offshore flow passes over the steep northern California orography; the resulting plume is advected offshore where its induced shallow circulation leads to flow reversal at the coast and stronger northerlies away from the coast.

There is no mechanism by which the offshore flow can generate PV frictionally within our idealized simulations, as the model is essentially inviscid (where the flow is smooth, i.e., away from the CTD leading edge) and adiabatic as the CTD develops, and there is no

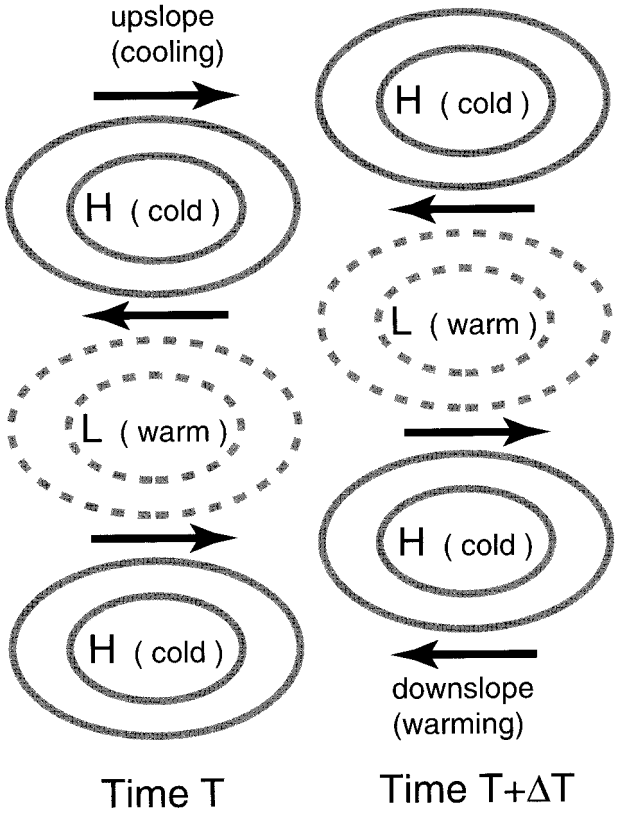

FIG. 13. Schematic representation of the propagation mechanism for topographically trapped Rossby waves. In the stratified atmosphere, downslope (upslope) flow causes warming (cooling) that leads to propagation of the pattern.

surface friction in the simulations. The evolution observed in the simulations can be understood in terms of PV conservation; within our simulations PV is generated only through diffusional processes, which only become significant after the CTD has already formed. Thus the simulations demonstrate that frictional generation of PV is not necessary for the production of a CTD.

5. Summary

A summary of CTD evolution, presented in Fig. 17, depicts qualitatively the evolution in the reference case simulation shown in Figs. 4 and 5. Before the CTD event, the climatological base state consists of high pressure in the north-central Pacific and a sloping marine layer accompanied by a northerly jet that has its maximum amplitude at the coast, where the marine layer, at its lowest point, intersects the coastal mountains. This state is depicted in the first panel of Fig. 17 at time t_0. The second panel, at time t_1, shows the early stage of the CTD event that begins with the eastward movement of the north-central-Pacific high onshore in the Pacific Northwest, possibly accompanied by westward movement of southwest U.S. low. This synoptic evolution produces offshore flow and also produces a mesoscale

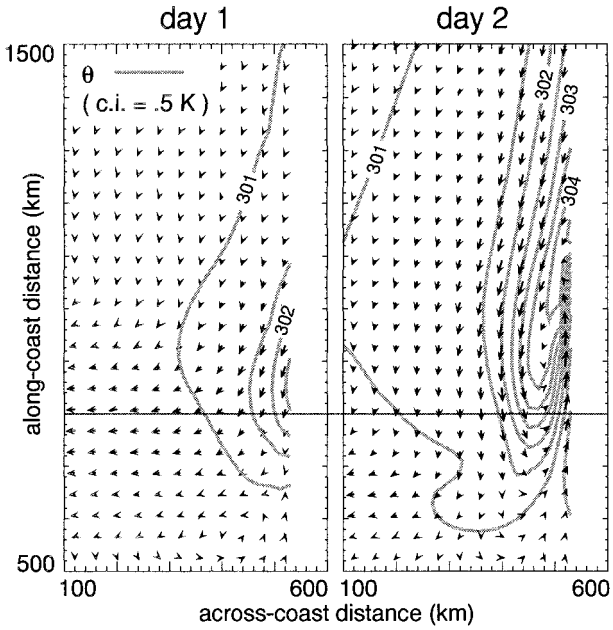

FIG. 14. Horizontal cross sections at $z = 300$ m for the simulation using a constant stratification ($N = 10^{-2}$ s^{-1}) with no marine layer. The centerline of the imposed offshore flow is also plotted.

coastal low by evacuation of the marine layer and lee troughing. As the low-level flow comes into geostrophic balance with the mesoscale low, the westerly flow to the south of the low encounters the coastal mountains and raises the marine layer. The increased pressure accelerates the flow northward along the coast. This elevated marine layer propagates to the north as a trapped disturbance (Fig. 17c at time $t = t_2$) into a region where the marine layer has been pushed offshore, producing coastal southerlies, and the coastal low becomes elongated and is displaced offshore.

Numerical simulations, using an idealized climatological mean state and forced by an imposed offshore flow of limited along-coast extent, reproduce the principal observed features of CTDs as described above in

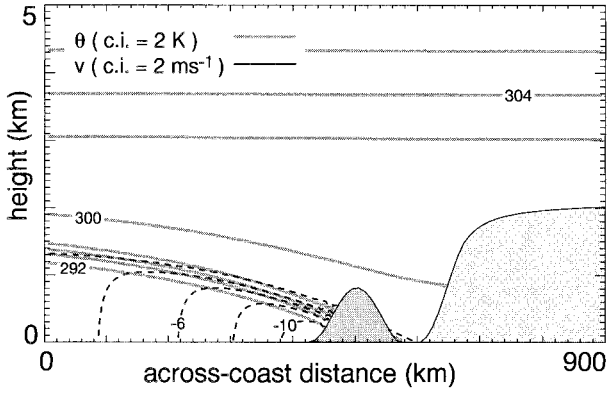

FIG. 15. Idealized climatological basic state with idealized California topography. Negative contours are dashed.

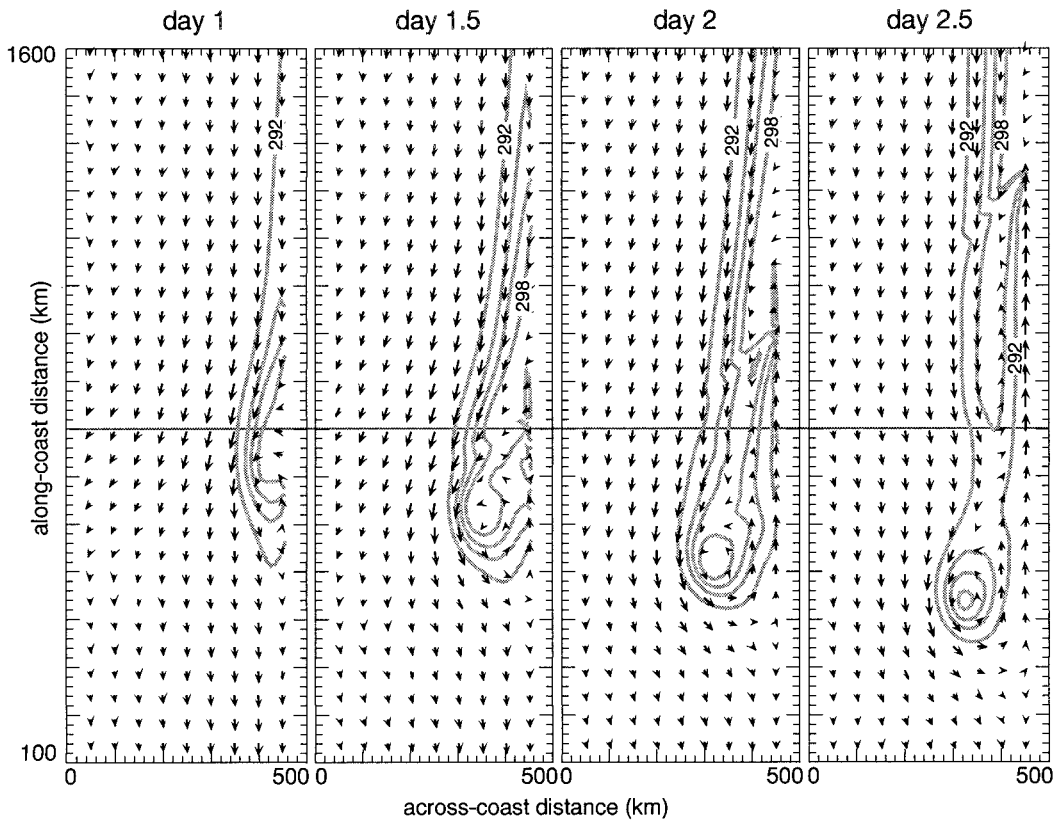

FIG. 16. Horizontal cross sections at $z = 300$ m from the simulation using the topography in Fig. 15. Potential temperature is contoured in gray (c.i. = 2 K) and the maximum velocity vector is approximately 16 m s^{-1}. The coastal mountains intersect the plane at $x = 460$ km. The centerline of the imposed offshore jet at $y = 800$ km is denoted by the thin line. The jet extends from 500 to 1100 km.

the summary (Fig. 17). The simulations also illuminate important dynamical features in CTD events. Two-dimensional (across coast) simulations show that rotation is crucial for offshore migration of the marine layer and northerly jet when offshore flow is imposed; in the absence of rotation the flow rides over the marine layer. Formation of the coastal mesoscale low pressure, amplification of the offshore migrating northerly jet, and appearance of coastal southerlies (observed features accompanying CTDs) are also found in the 2D simulations; these features are amplified by increasing stratification above the marine layer and increasing the height of the coastal topography. Three-dimensional simulations that include upper-level (above the marine layer) stratification show evidence of other observed CTD-related signals, including deep coastal southerly winds above the CTD and propagating surface pressure features both at the coast and farther inland. The southerlies above the CTD are in part produced by circulation about the coastal mesoscale low, and this coastal low strengthens with increasing stratification and with increasing mountain heights, as expected from linear theory.

There is evidence in the simulations that topographically trapped Rossby waves are responsible for the propagating pressure features outside the marine layer. These Rossby waves can significantly affect CTD evolution. The waves begin propagating to the north prior to CTD formation, and the accompanying flow opposes the offshore flow imposed by the synoptic-scale evolution. This opposition results in smaller offshore displacement of the marine layer and northerly jet, and inhibits the offshore movement of the coastal low later in the CTD evolution. The CTDs propagate faster with increasing stability above the marine layer, but we find that stronger offshore flows are required to initiate CTDs in the simulations because of the opposing circulation from the Rossby wave. The Rossby wave produces significant surface pressure perturbations that, given sufficient atmospheric stability relative to the marine layer depth and inversion strength, can be larger than those associated with elevation changes of the marine layer.

Propagating modes that resemble CTDs can be produced in simulations without the presence of a marine layer, if there exists sufficient stratification. While these modes begin as propagating topographically trapped Rossby modes, they evolve nonlinearly to produce strong along-coast southerlies. Since the climatology does not exhibit strong stratification existing above the

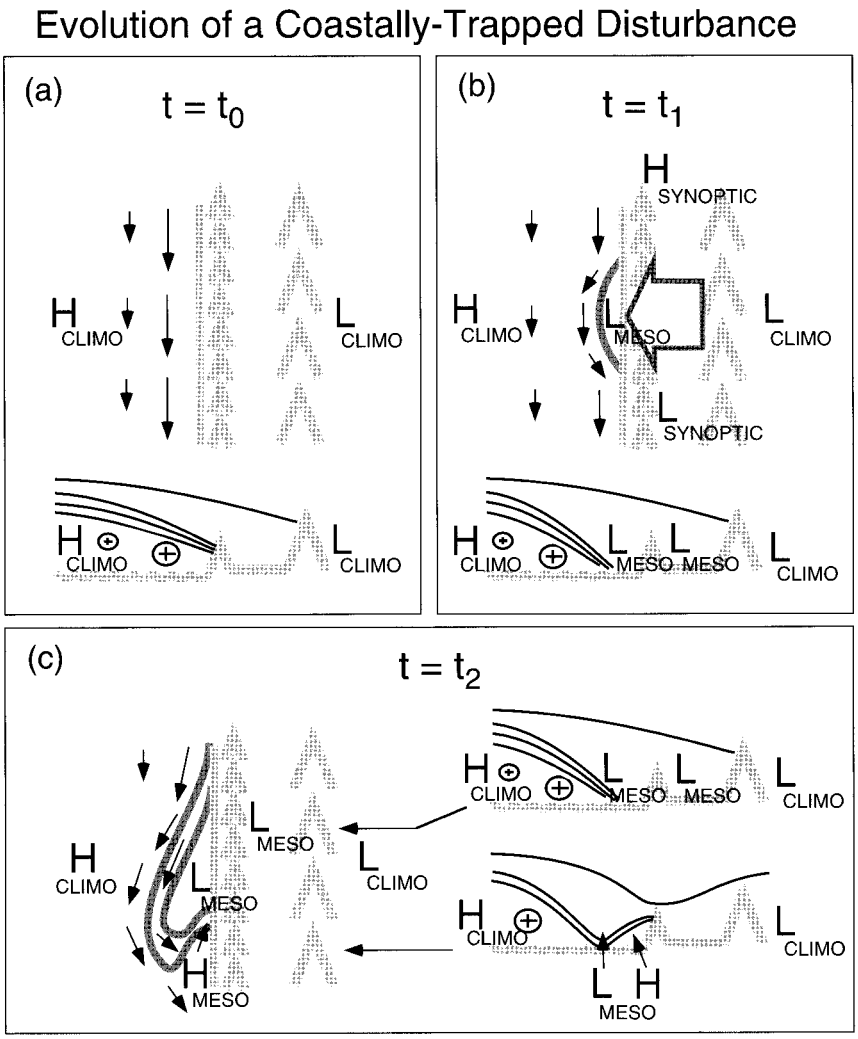

FIG. 17. Summary of coastally trapped disturbance evolution.

marine layer, we believe that these modes are not important for most observed U.S. west coast CTDs.

We interpret the CTDs in these simulations as being freely propagating disturbances once they are initiated by the local deepening of the marine layer by onshore flow to the south of the coastal low produced by the offshore flow. This interpretation is based on the fact that this region of local deepening does not propagate with the CTD, but rather stays fixed. A Rossby wave can produce onshore flow (that locally raises the marine layer) that propagates to the north. In our simulations this produces local accelerations in the southerlies well behind the leading edge of the CTD. However, the leading section of the CTD is still a freely propagating disturbance.

In our simple idealization, we have excluded a number of effects that may influence observed CTD evolution. We include a marine layer, but we do not include either the mechanisms for maintaining it (sea surface fluxes) or mechanisms for eroding it (radiation, diurnal processes, etc.). For example, our simulations show an almost complete removal of the marine layer in the region of offshore flow, but sea surface fluxes may prevent its complete removal and delay CTD evolution to a gravity current or bore. Our simulations do not contain any complex vertical structure in the inversion, structure that might depend on surface friction, diurnal effects, or other more complicated forcing. We examine only a smooth coastal plateau, with no along-coast variations, and only the case where offshore flow is perpendicular to the coast. The actual coastal mountain topography likely leads to significantly altered structure in the propagating CTD; and differing offshore flow structure, interacting with more realistic topography, may strongly influence CTD initiation and evolution. Also, we do not include surface heating over the land paralleling the boundary layer heating in the southwestern desert; advection of this heated air may be significant in producing or enhancing the coastal mesoscale low in some CTD events.

Acknowledgments. This research is supported in part by the Office of Naval Research Grant N00014-97-1-0013.

APPENDIX

For the climatological mean state depicted in Fig. 1, described in an (x, z) coordinate system, where x is the across-coast dimension, z is the height, and $x = 0$ corresponds to the left boundary of the computational domain, the potential temperature, including the sloping marine inversion, is given by

$$\theta(x, z) = \overline{\theta}(z) + \frac{\Delta\theta}{2}\left[\frac{2}{\pi}\tan^{-1}\left(\frac{z - z_{\text{inv}}(x)}{\Delta Z}\right) - 1\right],$$

where $\overline{\theta}(z)$ is the mean potential temperature profile and $\Delta\theta$ is the potential temperature difference across the inversion. The mean inversion height is given by

$$z_{\text{inv}}(x) = 2000\frac{2}{\pi}\tan^{-1}\left(\frac{x_c - x}{L_{\text{inv}}}\right) \text{m}.$$

The wind field in geostrophic balance with this potential temperature field is

$$v(x, z) = \frac{\Delta\theta g}{\pi\overline{\theta}(z)f}\frac{2000}{L_{\text{inv}}}\left[1 + \left(\frac{x - x_c}{L_{\text{inv}}}\right)^2\right] \times \left[\frac{2}{\pi}\tan^{-1}\left(\frac{z - z_{\text{inv}}(x)}{\Delta Z}\right) - 1\right]. \quad \text{(A1)}$$

The parameters for the state given in Fig. 1 are $x_c = 580$ km, $L_{\text{inv}} = 300$ km, $\Delta Z = 100$, $\Delta\theta = 10$ K, $f = 10^{-4}$ s^{-1}, and $g = 9.81$ m s^{-2}. Several mean potential temperature profiles are used in this study. Depicted in Figs. 1 and 15 is our climatological θ profile,

$$\overline{\theta}(z) = \theta_0 + 10^{-5}\frac{\theta_0}{g}z \qquad \text{for } z < 2500 \quad \text{(A2)}$$

$$\overline{\theta}(z) = \theta_0 + 10^{-5}\frac{\theta_0}{g}2500 + 10^{-4}\frac{\theta_0}{g}(z - 2500) \quad \text{for } z > 2500, \quad \text{(A3)}$$

with $\theta_0 = 300$ K. We also use a constant lapse rate profile $\overline{\theta}(z) = \theta_0 + 10^{-4}(\theta_0/g)z$ and a neutral profile $\overline{\theta}(z) = \theta_0$ in some simulations.

The idealized terrain depicted in Fig. 1 represents the flat ocean ($x < 500$ km), a constant slope between $x = 500$ km and $x = 700$ km, followed by a flat plateau of height $z = 1500$ m for $x > 700$ km.

The more realistic idealized terrain of Fig. 15 represents the California coastal range and the Sierras farther to the east. For the coastal range, the terrain height rises from sea level to approximately 800 m over approximately 50 km and the largest slope is slightly less than 1/50. The Central Valley lies between the coastal range and the Sierras, and our idealization of the Sierras has them rising from the valley (at sea level) to slightly over 2 km, with most of the elevation gain occuring over the first 100 km (from the valley, between 150 to 250 km from the coast).

The height of the terrain in Fig. 15 can be expressed as

$$H = H_0\left[\frac{1}{2} + \frac{1}{\pi}\tan^{-1}\left(\frac{x_s}{L_s}\right) + \frac{7}{20}\cos^2\left(\frac{\pi}{2}\frac{x_c}{L_c}\right) - \frac{3}{20}\cos^2\left(\frac{\pi}{2}\frac{x_v}{L_c}\right)\right] - 100 \text{ m}, \quad \text{(A4)}$$

where $x_s = x - 650$ km, the midpoint of the Sierra rise is at $x_s \sim 0$,

$$x_c = \min[-L_c, \max(L_c, x - 500 \text{ km})],$$

the peak of the coastal range is at $x_c \sim 500$ km, and

$$x_v = \min[-L_c, \max(L_c, x - 605 \text{ km})].$$

The term associated with x_v in (A1) is used to bring the elevation of the Central valley down to sea level. The terrain height H is set to zero where $H < 0$. The length scales defining the Sierra half-width, the coastal range width, the inversion thickness, the inversion half-width, and the temperature jump are $L_s = 30$ km, $L_c = 150$ km, $\Delta Z = 100$ m, $L_{\text{inv}} = 300$ km, and $\Delta\theta = 10$ K, respectively.

REFERENCES

Bond, N. A., C. F. Mass, and J. E. Overland, 1996: Coastally trapped wind reversals along the United States west coast during the warm season. Part I: Climatology and temporal evolution. *Mon. Wea. Rev.*, **124,** 430–445.

Dorman, C. E., 1985: Evidence of Kelvin waves in California's marine layer and related eddy generation. *Mon. Wea. Rev.,* **113,** 827–839.

——, 1987: Possible role of gravity currents in northern California's coastal summer wind reversals. *J. Geophys. Res.*, **92,** 1497–1506.

——, 1997: Comments on ''Coastally trapped wind reversals along the United States west coast during the warm season. Part II: Synoptic evolution.'' *Mon. Wea. Rev.*, **125,** 1692–1694.

Durran, D. R., 1995: Do breaking mountain waves decelerate the local mean flow? *J. Atmos. Sci.*, **52,** 4010–4032.

——, and J. B. Klemp, 1983: A compressible model for the simulation of moist mountain waves. *Mon. Wea. Rev.*, **111,** 2341–2361.

Gill, A. E., 1977: Coastally trapped waves in the atmosphere. *Quart. J. Roy. Meteor. Soc.*, **103,** 431–440.

Klemp, J. B., and R. Wilhelmson, 1978: The simulation of three-dimensional convective storm dynamics. *J. Atmos. Sci.*, **35,** 1070–1096.

Mass, C. F., and M. D. Albright, 1987: Coastal southerlies and alongshore surges of the west coast of North America: Evidence of mesoscale topographically trapped response to synoptic forcing. *Mon. Wea. Rev.*, **115,** 1707–1738.

——, and ——, 1988: Reply. *Mon. Wea. Rev.*, **116,** 2407–2410.

——, and N. A. Bond, 1996: Coastally trapped wind reversals along the United States west coast during the warm season. Part II: Synoptic evolution. *Mon. Wea. Rev.*, **124,** 446–461.

——, and N. A. Bond, 1997: Reply. *Mon. Wea. Rev.*, **125,** 1695–1697.

Neiburger, M., D. S. Johnson, and C.-W. Chien, 1961: *Studies of the Structure of the Atmosphere over the Eastern Pacific Ocean in the Summer*. University of California Press, 94 pp.

Persson, P. O., P. J. Neiman, and F. M. Ralph, 1995: Topographically generated potential vorticity anomalies: A proposed mechanism for initiating coastally trapped disturbances. Preprints, *Seventh Conf. on Mountain Meteorology*, Breckenridge, CO, Amer. Meteor. Soc., 216–222.

Pierrehumbert, R. T., 1984: Linear results on the barrier effects of mesoscale mountains. *J. Atmos. Sci.*, **41,** 1356–1367.

Ralph, F. M., L. Armi, J. M. Bane, C. Dorman, W. D. Neff, P. J. Neiman, W. Nuss, and P. O. G. Persson, 1998: Observations and analysis of the 10–11 June 1994 coastally trapped disturbance. *Mon. Wea. Rev.*, **126,** 2435–2465.

Reason, C. J., and D. G. Steyn, 1992: The dynamics of coastally trapped mesoscale ridges in the lower atmosphere. *J. Atmos. Sci.*, **49,** 1677–1692.

Rhines, P., 1970: Edge-, bottom-, and Rossby waves in a rotating stratified fluid. *Geophysical Fluid Dynamics*, A. R. Robinson, Ed., Vol. 1, Gordon and Breach Science, 273–302.

Rogerson, A. M., and R. M. Samuelson, 1995: Synoptic forcing of coastal-trapped disturbances in the marine atmospheric boundary layer. *J. Atmos. Sci.*, **52,** 2025–2040.

Thompson, W. T., T. Haack, J. D. Doyle, and S. D. Burk, 1997: A nonhydrostatic mesoscale simulation of the 10–11 June 1994 coastally trapped wind reversal. *Mon. Wea. Rev.*, **125,** 3211–3230.

Williamson, L. D., and P. J. Rasch, 1989: Two-dimensional semi-Lagrangian transport with shape-preserving interpolation. *Mon. Wea. Rev.*, **117,** 102–129.

Zemba, J., and C. A. Friehe, 1987: The marine atmospheric boundary layer jet in the coastal ocean dynamics experiment. *J. Geophys. Res.*, **92,** 1489–1496.